

***s*-orbital continuum model accounting for the tip shape in simulated scanning tunneling microscope images**

Roberto Gaspari,^{*} Stephan Blankenburg, Carlo A. Pignedoli, Pascal Ruffieux, Matthias Treier,[†]
Roman Fasel,[‡] and Daniele Passerone[§]

Empa, Swiss Federal Laboratories for Materials Science and Technology, Überlandstrasse 129, 8600 Dübendorf, Switzerland

(Received 13 May 2011; revised manuscript received 26 July 2011; published 8 September 2011)

In this paper we present a simple method accounting for tip size effects in scanning tunneling microscopy (STM) simulations. We consider the case where the tip atoms can be regarded as independent sources of *s* orbitals and compute the tunneling current using the Bardeen formula and the approximation of incoherent scattering. By averaging over the many possible tip configurations compatible with the effective external shape of the STM probe, we show that the tunneling current is proportional, within our model, to the convolution product between the local density of states of the system and a three-dimensional step function defined by the effective tip volume. The method is tested on three systems of current scientific interest, namely, a hexabenzocoronene molecule adsorbed on Cu(111), a reconstructed Au(677) surface, and a formate molecule adsorbed on Pt(111), which we study by means of large-scale density functional theory calculations and STM experiments. An excellent agreement between experimental and simulated STM images is found. It is shown that, under typical experimental conditions, our approach recovers the results of the well-known Tersoff-Hamann modeling in the case of spherical tips, while allowing for more versatility in the choice of the shape of the STM probe. Finally we present an application of our method to one-dimensional surface models mimicking a localized defect and a surface step, thereby offering a very simple framework for the discussion of the tip-induced broadening of the surface features in the STM imaging.

DOI: [10.1103/PhysRevB.84.125417](https://doi.org/10.1103/PhysRevB.84.125417)

PACS number(s): 68.37.Ef, 02.70.-c, 68.35.B-, 31.15.A-

I. INTRODUCTION

Scanning tunneling microscopy (STM) can produce atomic-resolution images of metallic or semiconductor surfaces, using the principle of quantum tunneling of electrons between a metallic tip and the scanned surface. In a remarkable review by Gottlieb and Wesolowski¹ the first experiments with STM are reconsidered, and Au(111) is cited as an example where STM can investigate different length scales: from the herringbone reconstruction, through imaging surface standing waves of electronic density induced by a defect, down to the individual gold atoms. The tunneling current depends on the atomistic structure of the STM probe. Although reasonable atomistic models of the STM tip already exist, its explicit geometry remains basically unknown during the STM experiments. Taking inspiration from the simple situation where a tip terminated with a single atom approaches a flat surface, it is tempting to conclude that the electronic structure in the vicinity of the tip apex atom will always overwhelmingly determine the tunneling current, due to the fact that the probability of tunneling through a high barrier decreases exponentially with the width of the barrier. But, as we will see below, reducing the tip to a single contributing “atom” is not always satisfactory, particularly when the corrugation of the surface is comparable to the tip curvature, as in the case of molecular adsorbates or surface steps. In these cases, several atoms of the tip can be at equivalent distances from the surface to be imaged, and a model taking into account the real size of the STM tip is needed.

Most simplified models for computing the STM current are derived from Bardeen’s theory,² which was published well before the invention of STM. Bardeen’s theory is adequate when the tip and the sample are sufficiently far apart and

when the potential between tip and sample is low enough. The derivation of Bardeen’s theory, beautifully sketched in Ref. 1, is a perturbation approach starting from the available information about the tip and the sample separately and then studying the scattering of tip states into sample states or vice versa. This approach leads to a formula for the tunneling current, which can be further simplified in the case of low temperature and/or low bias. Moreover, the matrix elements involved in the tunneling current can be computed by performing a flux integral on any surface belonging to a suitably defined barrier region.^{3,4} One road for simplifying the computation of the tunneling current is to treat the tip structure using simple idealizations, as in the well-known Tersoff-Hamann (TH) model.⁵ The TH model is derived from Bardeen’s formula under the assumption that the tip can be modeled as a spherical potential well. The tip eigenstates are the spherical Bessel functions, describing solutions associated with different angular momenta. The TH model retains only the smallest angular momentum component $l = 0$, corresponding to an *s* wave. Within this approximation the STM image is a contour of the local density of states (LDOS) of the system. This very simple result gives a straightforward framework for the interpretation of STM experiments, which can be related to a physical property of the sample alone. The contribution of the tip to the STM image is given only by the radius of the spherical tip which sets the intensity of the current and therefore the average tip-sample separation at which the imaging is performed. Within the TH model, the tip is modeled as a protruding piece of Sommerfeld metal and tip electrons are delocalized entities within the well. By taking the opposite perspective, Chen⁶ interpreted the tip states as dominated by one single atomic orbital localized on the outermost atom of the tip and developed a

formalism to include $l > 0$ corrections to the tip states in the calculation of the tunneling matrix elements. For tips dominated by one single s orbital, the atomistic interpretation recovers the result of TH and the STM image is represented by a contour of the LDOS at the Fermi level E_f . Even for the $l = 0$ case, however, the two pictures cannot be considered equivalent: while the TH approximation takes into account the size of the tip, modeling the tip states as a single s orbital corresponds to the use of a pointlike tip and does not allow reproduction of the tip-induced smearing of the surface features. By keeping the atomistic point of view, a remedy to this limitation would be the use of models accounting for tips composed of many atoms. However, the atomistic structure of the tip is normally unknown and, if it were available, more accurate ways to compute the tunneling current would be then at hand.^{3,4} Therefore it would be valuable to have tip models based on an atomistic description but at the same time requiring only reduced information on the tip structure, such as its effective outer shape. The aim of this paper is to propose a STM simulation method that effectively takes into account the size of the STM tip, starting from an atomistic description of the tip itself. We consider tips composed of a large number of atoms and model the tip states as a linear combination of atomic orbitals. By using the Bardeen formula, we compute the tunneling current in the incoherent sum approximation and, within this approximation, obtain an expression which is valid for an arbitrary arrangement of tip atoms. By averaging the current value over many tip configurations which are bound by a particular tip shape, we show that the resulting current intensity is proportional to the convolution product of the system LDOS with a step function defined by the effective tip volume. This simple result allows for a conceptual framework where tip size effects can be understood in a straightforward manner. We show that, under typical experimental conditions and in the case of spherical tips, our approach is equivalent to the TH model. However, our method allows us to simulate STM images using tips of *any* shape at a very moderate computational cost, which differs negligibly from that demanded by the TH modeling. We named our tip model the “ s -orbital continuum” (SOC) model, since it corresponds eventually to a continuum of atomic orbitals bound by the tip surface, and in this work we considered only tips composed of atoms with dominant s -orbital character.

II. MATERIALS AND METHODS

Electronic structure calculations were performed in the framework of density functional theory (DFT) using the mixed Gaussian–plane wave basis set approach implemented in CP2K.⁷ Kohn-Sham equations were solved using the Perdew-Burke-Ernzerhof exchange correlation functional, Goedecker-Teter-Hutter pseudopotentials, and contracted Gaussian basis sets⁸ for all elements. The Poisson equation was solved by expanding the charge density in plane waves using a cutoff of 280 Ry. In order to study the properties of a model tip, we calculated the electronic structure of a system composed of a small cluster of gold on one monolayer of Au(111). The periodic unit cell is orthorhombic, the cell size is $35 \times 35 \text{ \AA}^2$ along the monolayer plane and 60 \AA in the perpendicular direction. We then investigated three systems of current

scientific interest, an isolated hexaperihexabenzocoronene (HBC, $C_{42}H_{18}$) molecule adsorbed on Cu(111), a stepped Au(677) displaying surface reconstruction, and a formate molecule (HCO) adsorbed on Pt(111). The details of the Au(677) calculation have been reported elsewhere.⁹ However with respect to Ref. 9, the calculation was repeated using a kink-free slab. The HBC/Cu(111) calculations were performed using an orthorhombic cell. The cell size is $40 \times 41 \text{ \AA}^2$ along the surface plane and 60 \AA in the perpendicular direction. The system contains one HBC molecule adsorbed on a slab of five layers of copper and one additional layer of hydrogen deposited on the deepest copper layer. This allows us to suppress one of the two surface states^{10,11} arising in a Cu(111) slab calculation, thus removing possible artifacts due to the finite thickness of the slab.^{12,13} Dispersion forces in the HBC/Cu(111) system were taken into account using the empirical parametrization of Grimme.¹⁴ The two deepest layers of the Cu slabs were kept fixed to bulk positions and structural optimization was performed until the largest forces on atoms were as small as 10^{-4} a.u. The electronic optimization of the Au(677) and Cu(111) surfaces was repeated after structural optimization using additional Gaussian basis functions centered 2 \AA above each surface atom. This ensures more variational freedom in the calculations of the surface wave function in vacuum and therefore a better description of the Kohn-Sham states up to the beginning of the vacuum region.¹⁵ The HCO/Pt(111) system was optimized using a unit cell of size $22.4 \times 19.4 \text{ \AA}^2$ along the surface plane and 60 \AA in the perpendicular direction. The slab used consists of six layers of Pt(111). The structural optimization was carried out analogously to the case of HBC/Cu(111). After the electronic optimization was carried out, the individual states were analytically extrapolated into the vacuum region using the matching procedure described in Refs. 16–18. STM experiments were performed on a low-temperature STM (Omicron Nanotechnology) with a base pressure of 10^{-10} mbars. Cu(111) was prepared by repeated argon ion bombardment and annealing to 800 K. HBC molecules were deposited from a resistively heated quartz crucible at $1 \text{ \AA}/\text{min}$ with the substrate kept at room temperature. STM images were recorded at 5 K. Details of the experimental measurements for the Au(111) stepped surface are reported in Ref. 9.

III. DESCRIPTION OF THE METHOD

The Tersoff-Hamann approximation⁵ is obtained from the Bardeen formalism² under the assumption that the tip can be modeled as a spherical potential well. The Bardeen formalism states that the tunneling current depends on the following integral:

$$I = \frac{2\pi e}{\hbar} \sum_{\mu,\nu} f(E_\mu)[1 - f(E_\nu + eV)] |M_{\mu\nu}|^2 \delta(E_\nu - E_\mu), \quad (1)$$

where $f(E)$ is the Fermi function, V is the applied voltage, $M_{\mu\nu}$ is the tunneling matrix element between states ψ_μ of the probe and ψ_ν of the surface, and E_μ is the energy of state ψ_μ in the absence of tunneling. The explicit formula for the the matrix element reads

$$M_{\mu\nu} = \frac{\hbar^2}{2m} \int d\vec{S} \cdot (\psi_\mu^* \vec{\nabla} \psi_\nu - \psi_\nu \vec{\nabla} \psi_\mu^*) \quad (2)$$

and the surface integral is performed on a separation surface, which can be any surface lying entirely in the vacuum region. The TH approximation models the tip as a macroscopical spherical well, whose eigenstates are spherical Bessel functions corresponding to different angular momenta. In their description, Tersoff and Hamann retained only the $l = 0$ component and showed that, in the limit of low temperatures and low bias voltages, the matrix element $M_{\mu\nu}$ is proportional to the value of the sample state $\psi_\nu(\vec{r}_0)$, \vec{r}_0 being the center of the well. As a result the current intensity recorded by the STM tip is proportional to the LDOS of the sample at \vec{r}_0 , at the Fermi energy E_f :

$$I(\vec{r}_0) \propto \sum_\nu |\psi_\nu(\vec{r}_0)|^2 \delta(E_\nu - E_f) = \rho(E_f, \vec{r}_0), \quad (3)$$

where ψ_ν are the one-electron states of the investigated sample and E_ν are the corresponding one-electron energy levels. In describing the tip structure as a macroscopic potential well, the theory of TH does not explicitly refer to the atomistic structure of the tip and to the individual atomic states from which the tip eigenfunctions are derived. Rather it models the tip electrons as delocalized entities within the well. By taking the opposite perspective, Chen⁶ interpreted the tip states as dominated by one single atomic orbital localized on the outermost atom of the tip and developed a formalism to include $l > 0$ corrections to the tip states in the calculation of the tunneling matrix elements. For tips dominated by one single s orbital, the atomistic interpretation recovers the result of TH, and the STM image is represented by a contour of the LDOS at E_f . Even for the $l = 0$ case, however, the two pictures cannot be considered equivalent: while the TH approximation takes into account the size of the tip, modeling the tip states as a single s orbital corresponds to a pointlike tip. The tip size effect in the TH approximation is accounted for by the fact that LDOS contours are taken at the center of the well, rather than at the tip bottom. As a remark, we use the term *s wave* when referring to the $l = 0$ eigenstate of a macroscopic potential well, as in the TH approximation, while the term *s orbital* is instead used in the context of the atomistic interpretation of the tip. In Fig. 1 we present an example calculation in order to gain more insight into the actual electronic features of a realistic tip, using *ab initio* calculations as described in the previous section. The tip is represented as a cluster of gold atoms on a Au(111) monolayer. The cluster was obtained from the gold bulk structure by selecting only atoms falling within a hemisphere of 9 Å radius and with base parallel to the [111] plane. Since there are many ways to obtain a cluster of gold atoms contained in such an hemisphere, we chose a cluster terminated by a single atom, therefore mimicking a realistic tip able to yield high-resolution images. In Fig. 1 we show the contour profile of the eigenstates of the system at E_f (in practice we averaged the amplitude of states over a small energy window of 0.1 eV below E_f). The isovalue ($10^{-4} e/\text{Å}^3$ for the corresponding density of states) was chosen so as to be closest to a hypothetical spherical wave front that is at 3 Å distance from the tip surface. It is noticeable that, locally, below the tip apex atom, the tip states can be very well represented by a single s orbital originating from the tip atom itself. In the imaging of a flat surface only the shape of the tip states below the apex atom is relevant, and the

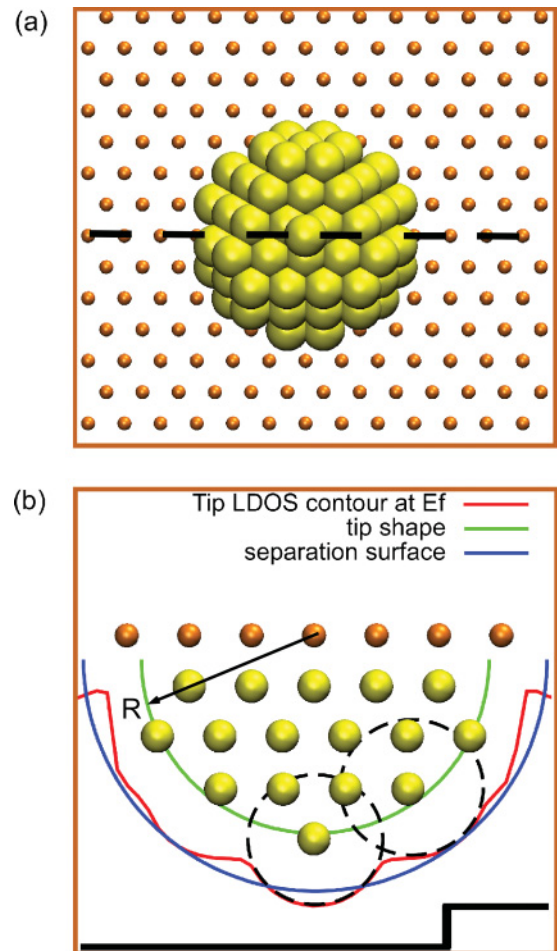


FIG. 1. (Color online) (a) Top view of the gold cluster bounded by a hemispherical volume of $R = 9 \text{ \AA}$ radius. Smaller atoms represent the Au(111) layer supporting the cluster. (b) Section of the cluster along the dashed line in (a). The inner circle represents the cluster envelope; the outer circle is a spherical wave front 3 Å away from the tip surface. The thicker black line represents an ideal stepped surface. The tip state contour, at E_f , in the vacuum region across the step edge can be roughly approximated by a single s wave. A better description is obtained using two s orbitals (dashed circles) originating from the tip atom closest to the sample.

single- s -orbital approximation, for the particular case described here, works very well. However, if the STM tip is scanning across a corrugated surface, the picture of a single-atom-terminated tip breaks down, as several tip atoms can be equivalently distant from the surface to be imaged. In this case the overlap between the tip and sample states is significant over a larger portion of space, and the description of the tip states must be correct over the whole space of significant overlap. In the example depicted in Fig. 1 we see that a correct description of the tip states in the region of interest can be obtained by using two s orbitals, these waves being centered on the positions of the tip atoms closest to the sample. The example shows moreover that use of a single s wave originating from the center of the tip, as in the TH approximation, is a worse approximation of the real tip states at the Fermi level. In the following we show how to account for tip size effects using the atomistic interpretation, by computing the matrix element

(2) for a tip state composed of a combination of s orbitals. We describe the tip states as the following sum:

$$\psi_\mu(\vec{r}_0) = \sum_{k=1}^N e^{i\alpha_{k,\mu}} \phi(\vec{r}_k + \vec{r}_0), \quad (4)$$

similarly to what was proposed in Ref. 19, where $\psi_\mu(\vec{r}_0)$ is the tip state, \vec{r}_0 identifies the location of the tip during the scan (it can be, for example, the geometrical center of the many-atom tip), $\phi(\vec{r}_k + \vec{r}_0)$ is a generic s wave centered on the k th atom at R_k , R_k being expressed as the sum of \vec{r}_0 and the position \vec{r}_k

of the k th atom relative to the tip center, $\alpha_{k,\mu}$ is the phase of the k th orbital in the expansion of state ψ_μ , and the number of atoms ranges from 1 to N . Following the derivation of the matrix element $M_{\mu\nu}$ for the single s orbital as described in Ref. 6, the appropriate expression in our case reads

$$M_{\mu\nu} \propto \sum_{k=1}^N e^{i\alpha_{k,\mu}} \psi_\nu(\vec{r}_k + \vec{r}_0). \quad (5)$$

Taking the square of the the matrix element in (5) yields

$$I(\vec{r}_0) \propto \sum_{v,\mu} \left[\sum_k |\psi_v(\vec{r}_k + \vec{r}_0)|^2 + \sum_{k,j,k \neq j} e^{i(\alpha_{k,\mu} - \alpha_{j,\mu})} \psi_v(\vec{r}_k + \vec{r}_0) \psi_v^*(\vec{r}_j + \vec{r}_0) \right] \delta(E_v - E_f), \quad (6)$$

where we have separated the diagonal terms ($k = j$) and the off-diagonal terms ($k \neq j$). In order to simplify the expression above, we perform the sum in the incoherent approximation, by assuming that the off-diagonal terms cancel out due to the averaging of the many tip states.¹⁹ We do not consider here cases where the incoherent approximation is not appropriate, as in the case of tips with special geometries discussed in Ref. 20.

This leads to the following formula for the tunneling current:

$$I(\vec{r}_0) \propto \sum_{k=1}^N \rho(E_f, \vec{r}_k + \vec{r}_0). \quad (7)$$

In our simulations we compare with experiments performed at a finite bias V_b and we need to take into account the contributions from states away from the Fermi energy. In principle a finite bias V_b induces distortions of the electric potential across the junction and consequently modifies the tip and sample states. However, for values of the bias which are small with respect to the work functions of the tip and the sample, it is not unreasonable to consider the matrix element in (2) as bias independent.²¹ Keeping in mind these caveats, we can write the recorded current intensity as

$$\begin{aligned} I(\vec{r}_0) &\propto \sum_{k=1}^N \sum_{E_v \in [E_f - V_b; E_f]} |\psi_v(\vec{r}_k + \vec{r}_0)|^2 \\ &= \sum_{k=1}^N \bar{\rho}(\vec{r}_k + \vec{r}_0), \end{aligned} \quad (8)$$

where $\bar{\rho}$ is the LDOS integrated from $E_f - V_b$ to E_f . The value of V_b will be specified in the text for all cases treated. The precise position of the N tip atoms included in (8) depends of course on the tip shape and structure, which are not known *a priori*. We therefore model the tip as a volume Ω with a suitable geometric form (hemisphere, pyramid, etc.) and we compute the current as an average $\langle I(\vec{r}_0) \rangle$ over a set $\{C\}$ of different tip configurations, corresponding to atomic arrangements bound by the shape Ω . This gives

$$\langle I(\vec{r}_0) \rangle \propto \sum_{i \in \{C\}} \sum_{k=1}^{N_i} \bar{\rho}(\vec{r}_{k,i} + \vec{r}_0), \quad (9)$$

where $r_{k,i}$ is the k th atomic position of the i th configuration in $\{C\}$ relative to the tip center \vec{r}_0 . By averaging over a large number of configurations in $\{C\}$, the current in Eq. (9) can be approximated by the following expression:

$$\begin{aligned} \langle I(\vec{r}_0) \rangle &\propto \int_{\Omega} \bar{\rho}(\vec{r} + \vec{r}_0) d\vec{r} = \int s(\vec{r}) \bar{\rho}(\vec{r} + \vec{r}_0) d\vec{r} \\ &= \int s(\vec{R} - \vec{r}_0) \bar{\rho}(\vec{R}) d\vec{R} = g \star \bar{\rho}. \end{aligned} \quad (10)$$

By defining a step function $s(r)$, which is 1 when r is inside the volume Ω and 0 otherwise, the integral in Eq. (10) is evaluated over the whole space and finally reduces to a convolution product between the integrated LDOS and a shape function $g(r) = s(-r)$. Since many reasonable geometrical shapes are determined by a small number of parameters, our method allows a quick comparison to the experimental results. In the case of hemispherical tips, for instance, the only free parameter is the radius R of the tip. In our approximation the constant-current images reproduce isosurfaces of a convoluted LDOS (CLDOS) rather than contours of the bare LDOS. However, STM images simulated according to Eq. (10) become simple LDOS contours in two limiting cases, i.e., for small values of the tip radius and for large tip-sample distances. When the tip radius becomes very small the shape function $g(r)$ can be expressed as a Dirac delta function $\delta(r)$ and the convolution product in Eq. (10) simply gives the LDOS value at \vec{r}_0 . If the distance between the sample and the tip is large, the LDOS isolevels are approximately flat and the convolution with the shape function $g(r)$ keeps yielding flat images. Nonetheless, at smaller tip-sample distances convolution effects are expected to become important, especially for samples displaying corrugations of the order of Ω . From the computational point of view, convolution products can be evaluated in Fourier space using highly optimized routines for the Fourier transformation and do not produce any significant overhead with respect to the calculation of the bare LDOS isolevels. We note that the averaging over many tip configurations could have been performed directly on the current intensity computed in Eq. (6). This would lead to the averaging of the interference term, between atom k and atom j , not only on all the possible tip states but also on the various tip configurations with fixed number of atoms and occupied k and j positions, thus further

validating the assumption of incoherent scattering. Finally, the main result of our analysis could have been obtained also by directly computing the tunneling matrix element in the case of a uniformly and densely distributed set of tip atoms, which is why we named our tip model the *s*-orbital continuum model. It has to be noted that the model is not necessarily restricted to tips with *s*-orbital character but can be modified to account for higher-order-orbital angular momenta. When considering $l > 0$ atomic orbitals, the tunneling matrix elements involve spatial derivatives of the sample one-electron states.⁶ By substituting the appropriate expression of the matrix element in Eq. (2), it is possible to rederive Eq. (10) using the same procedure described for the *s*-orbital case, the LDOS function ρ being replaced by the square of the modulus of the corresponding matrix element. For example, in the case of d_{zx} orbitals the tunneling current would be proportional to the product $g \star \bar{\rho}_{d_{zx}}$, where $\bar{\rho}_{d_{zx}} = \sum_v |\partial^2 \psi_v / \partial z \partial x|^2$. This can have a direct application in the field of spin-polarized STM imaging, where the usual Cr or Fe tips display a strong *d*-orbital character.

The method described above takes into account the tip size effects for probes of arbitrary shape. This fact can be used to estimate the effective cross-sectional area of three-dimensional tips in a consistent way, which in turn creates a bridge to the one-dimensional theories of tunneling for the computation of the STM current. This clearly represents an advantage, since reducing the dimensionality leads to a more straightforward solution of the tunneling problem. In order to obtain the effective cross-sectional area of a spherical tip, we note that a flat electrode and a spherical tip, at the same distance from a flat surface, record the same current if their CLDOSs are equal, i.e., $\int_{\Omega_s} \bar{\rho}(z) d\vec{r} = \int_{\Omega_f} \bar{\rho}(z) d\vec{r}$, where Ω_s and Ω_f represent the volumes of the spherical and the flat electrode, respectively, and z is the distance from the surface. The formula above can be written for the explicit geometries of the planar and spherical tip [see (A1)], thus leading to a relationship $S(R)$ between the effective cross-sectional area of the tip, S , and its radius R . The value of S can be used to estimate the tunneling current in the one-dimensional models of tunneling. In our work we have used the tunneling theory of Simmons [metal-insulator-metal (MIM) model²²], which states that the current-distance characteristic across the junction, for small biases, reads

$$I = S \frac{\gamma \sqrt{\bar{\phi}} V_b}{\delta_z} e^{-A \delta_z \sqrt{\bar{\phi}}}, \quad (11)$$

where δ_z is the barrier width, $\phi(z)$ is the potential across the junction, $\bar{\phi}$ is the average value of the potential along the barrier width, V_b is the voltage between the electrodes, $\gamma = e \sqrt{2m(4\beta\pi^2\hbar^2)^{-1}}$, $A = 2\beta \sqrt{2m\hbar^{-2}}$, and $\beta = 1 - (8\bar{\phi}^2 \delta_z)^{-1} \int_{\delta_z} [\phi(z) - \bar{\phi}]^2 dz$. The barrier width δ_z is defined as the region between the crossing points of the electrode Fermi levels at $V = 0$ and the potential $\phi(z)$. A further explanation of the quantities involved in the calculation is given in Fig. 2. Since the tip is usually made after indentation into the substrate, it is not unreasonable to take the work function of the tip equal to that of the sample. This latter represents a very good estimate of $\bar{\phi}$. For our purposes the value of β can be approximated to 1. Finally, the value of

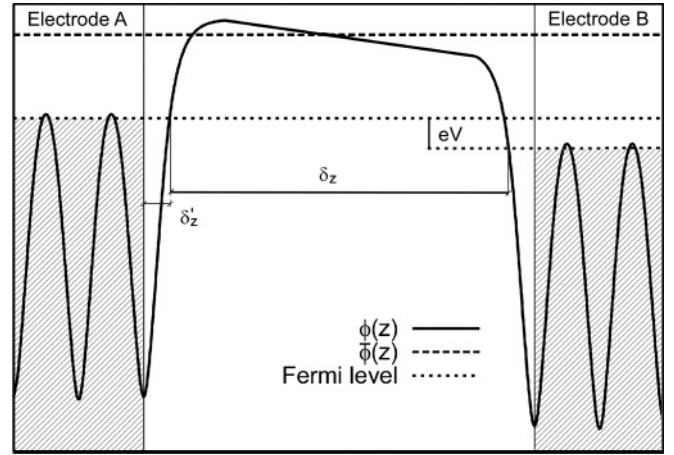


FIG. 2. The most important quantities involved in our MIM calculations. Details are reported in the text.

δ_z must be increased by a quantity δ'_z (see Fig. 2) if one is interested in the actual distance d between the electrode planes. In the cases of Cu(111) and Au(111) surfaces we found the value δ'_z to be between 0.7 and 0.8 Å. Assuming this value to be similar on both sides of the junction, δ_z should be increased by approximately 1.5 Å in order to get d . Once this latter value is obtained it is possible to compute the CLDOS of the spherical tip at the distance d from the substrate. The CLDOS value obtained represents the isosurface corresponding to the STM image using a convenient choice of the radius R and the experimental current and bias voltage as inputs.

IV. RESULTS

The method described in the last section will be used to explain experimental STM images of three systems of current interest, namely, a HBC molecule adsorbed on Cu(111), a reconstructed stepped surface of Au(111), and a HCO molecule adsorbed on Pt(111). These systems present large corrugations due to the presence of the steps and the adsorbed molecules and therefore can induce noticeable convolution effects in the STM imaging. These effects are quantified by comparison to simulations performed with pointlike tips.

A. HBC molecule

The large aromatic core of hexaperihexabenzocoronene ($C_{42}H_{18}$) represents an electron reservoir motivating the use of HBC-based molecules in molecular electronics. Jäckel *et al.* have shown that the use of HBC allows the building of a prototypical single-molecule chemical field-effect transistor.²³ The adsorption of HBC on Cu(111) below the monolayer coverage allows the investigation of single molecules with the help of STM. After geometry optimization the molecule reaches a planar configuration, about 2.8 Å above the surface. The Kohn-Sham states are matched to their exact asymptotic expression^{16–18} on the plane $z_c = 4.2$ Å above the Cu(111) substrate. The Kohn-Sham states decay in vacuum above the bare copper substrate, and the center of the HBC molecule is shown before and after asymptotic extrapolation in Fig. 3. The huge qualitative difference between the two cases proves the importance of an adequate treatment of the vacuum part

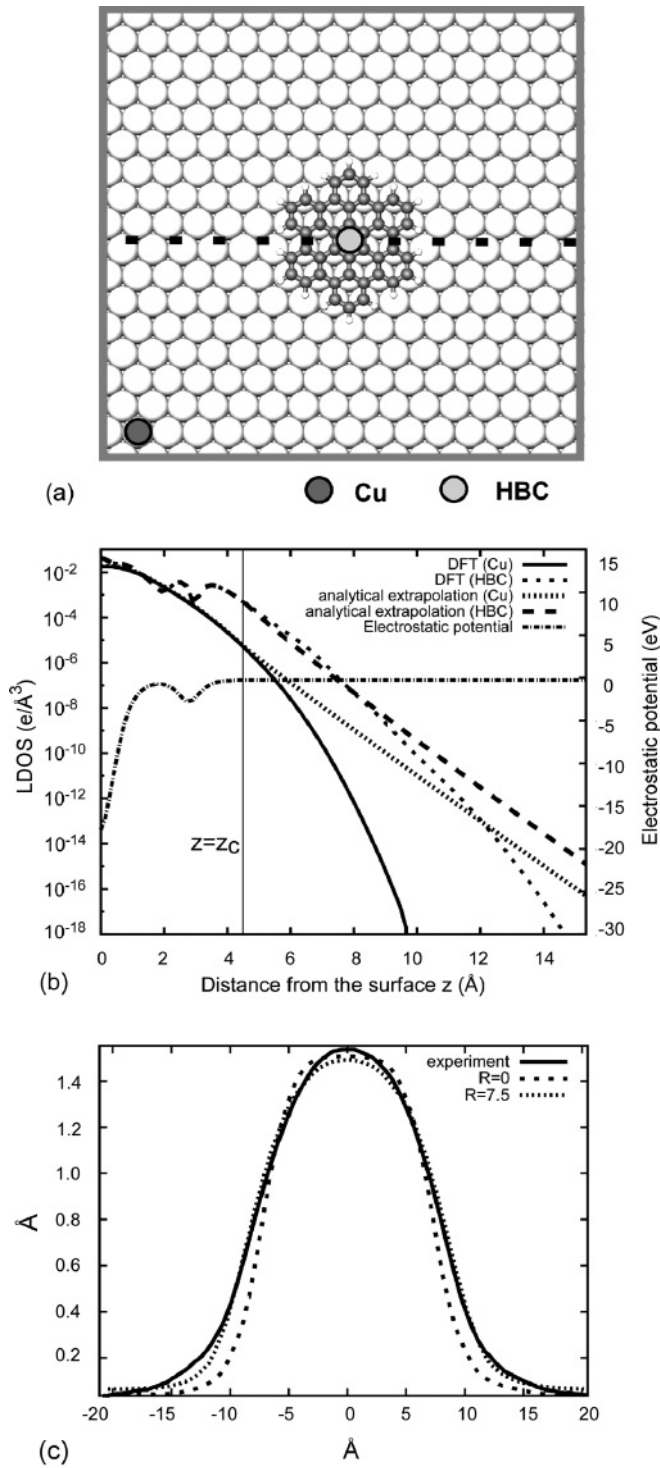


FIG. 3. (a) Top view of the HBC molecule on Cu(111). The dotted line indicates the direction of the STM scan. (b) The LDOS decay in vacuum above the Cu(111) substrate and the HBC molecule before and after analytical extrapolation of the sample states. The electrostatic potential profile represents an average over the plane parallel to the surface. (c) Experimental profiles together with the calculated profile obtained with an hemispherical tip of radius $R = 7.5 \text{\AA}$ and the same image after removing convolution effects ($R = 0 \text{\AA}$; see text for more details).

of the individual eigenstates, after DFT calculations using Gaussian or plane wave basis sets. In the following we compare simulated STM images to the experimental results. By using the relationship $S(R)$ derived in (A1) we obtain, for values of R between 3 and 9 \AA , an effective area ranging from 10 to 45 \AA^2 . These values can be used in the relationship (11) to estimate the tip-surface distance in our experiments. In the case of the bare Cu(111) surface, the experimental conditions given above correspond to a tip-sample distance (meant as the distance between the outermost nuclei of the electrodes) in a range between 6.5 \AA ($S = 10 \text{\AA}^2$) and 7.0 \AA ($S = 45 \text{\AA}^2$). In our STM simulations we computed the CLDOS isovalues on a copper atom far away from the HBC molecule, by requiring the tip-sample distance to be that predicted by the MIM model. Since LDOS isosurfaces correspond in our model to images taken with a pointlike $R = 0 \text{\AA}$ tip, the current cannot be compared to that obtained using a more realistic finite-size tip, like those used to reproduce the STM experiments presented in this paper. However, when calculating the appropriate CLDOS isovalue, we also computed the sample LDOS value at the bottom of the tip. The LDOS isosurfaces taken at that value represent the images that would be obtained by our STM model if convolution effects were discarded (single- s -orbital modeling) and bear therefore considerable information about the size effect of the tip in the imaging. In Fig. 3 we thus show the comparison between the simulated image according to our model using a tip with radius $R = 7.5 \text{\AA}$, the same image discarding convolution effects (LDOS isosurface, $R = 0 \text{\AA}$), and the experimental line profile. The LDOS isovalues appear in reasonably good agreement with the experimental result. However, at half maximum of the molecule, the width of the profile amounts to 16.3 \AA while the slope is 16.7° , corresponding respectively to increases of 9% and 33% with respect to the experimental value. Following these considerations, we conclude that convolution effects have to be taken into account in the explanation of this particular STM image. It is now interesting to look at the accuracy of taking the mean value of the current as expressed by Eq. (10). In order to check the validity of the mean value approximation we computed several STM images of the HBC molecule using tips that contain a finite number of atoms. In order to obtain the geometries of these tips we first chose the tip shape as the hemisphere of radius $R = 7.5 \text{\AA}$ used for the simulated STM image shown in Fig. 3. A given number of atoms were randomly scattered inside the tip volume so as to reach a realistic atomic density for a metallic structure (we chose the atomic density of bulk gold, i.e., 0.06 atoms/ \AA^3). In order to avoid unrealistic tip geometries, we constrained each atom to have a minimum neighbor distance of 2.5 \AA . 50 independent tip geometries were obtained in this way, and then used to generate a STM image by means of Eq. (8). The CLDOS was chosen so that each tip would stand about 6.75 \AA above the bare Cu(111) surface. The average width of the molecule, computed at the half-height of the profile, is 16.2 \AA with a standard deviation of 0.6 \AA , which corresponds to scarcely 3% of the average value. The small standard deviation confirms that the tunneling current averaged over several possible tip configurations as given by Eq. (10) is a robust representation

of the value that we would obtain from Eq. (8) if the actual tip structure were known.

B. Reconstructed Au(111) stepped surface

Stepped reconstructed surfaces of Au(111) have been studied in detail in previous work.⁹ In the following we review only the main aspects of the system. Large regions of flat Au(111) display the so-called herringbone phase, which is characterized on a smaller length scale by a uniaxial compression along a close-packed direction. Along the direction of compression 23 surface atoms occupy the same length spanned by 22 bulk atoms; hence the common name of $22 \times \sqrt{3}$ reconstruction. This compression gives rise to an alternation of bulk-terminated fcc regions and faulted hcp ones. When regular arrays of steps are introduced, such as in Au(788) or Au(677) (see Fig. 4), the long-range herringbone phase is lifted;²⁴ the uniaxial compression anyway still takes place leading to a reconstruction very similar to the $22 \times \sqrt{3}$ pattern. The presence of steps, however, slightly modifies the surface pattern which appears as an alternation of V-shaped domains, along the same terrace, containing hcp or fcc atoms. DFT calculations have shown that while step lines facing fcc domains are quite similar to a bulk termination, hcp ones display an unpredictable rearrangement: the step lines facing hcp regions are dramatically smoothed, and surface atoms from the lower and upper step edges coordinate so as to form a local close-packed surface, inclined by 28° with respect to the [111] direction. Experimental STM scans have been performed across the step at the hcp and fcc regions. The tip-sample distance was obtained by modeling the tip and the sample as two Au(111) electrodes and estimating their separation d in the same way as described in the previous section. The sample states were extrapolated in the vacuum region as described previously. For the STM simulations we computed the CLDOS isovalues above a gold atom in the open terrace, by requiring the tip-sample distance to be that predicted by the MIM model. Similarly to the case of the previous section, we also computed the LDOS value at the bottom of the tip in order to remove convolution effects and perform single- s -orbital modeling. STM profiles across the hcp and fcc regions of the step, using a tip of radius $R = 2 \text{ \AA}$, precisely reproduce the experimental features of the gold step. Again the use of a tip with radius $R = 0 \text{ \AA}$ (single- s -orbital modeling) yields a reasonably good agreement with experimental results. However, the slope and the width of the step contour are slightly underestimated. The tip used in this case is very sharp and might represent a single atom adsorbed on a minimal support. This leads to smaller convolution effects than in the case of the HBC/Cu(111) system, where a larger tip was needed to match the experimental result.

C. HCO molecule on Pt(111)

In the previous sections we studied the effects of convolution under typical experimental conditions. It turns out that, in these cases, the tip-sample distance is quite large and that modeling the tip as a point already provides good results. This can be explained by the fact that, at large tip-sample distances, the LDOS isosurfaces are quite smooth and the convolution

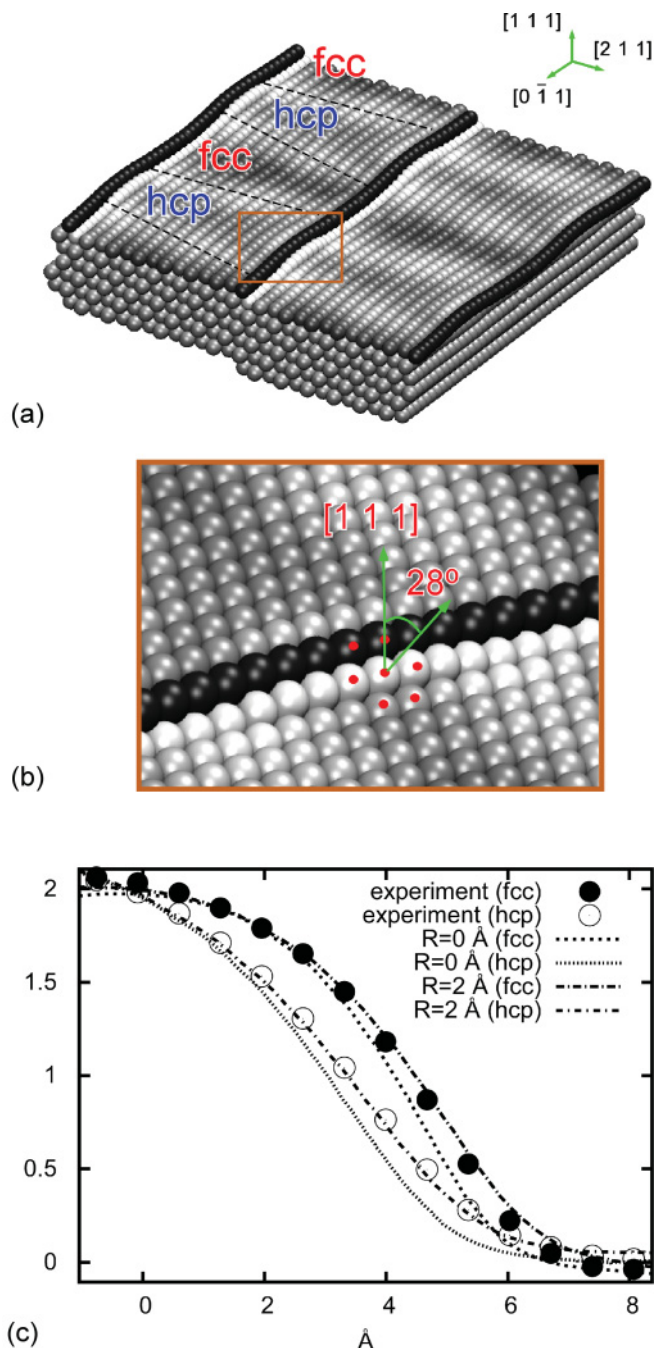


FIG. 4. (Color online) (a) Snapshot of the Au(677) surface model after DFT optimization. Gray levels are associated with the physical height of the atoms with respect to the terrace level. Brightest terrace regions correspond to the protruding discommensuration lines and separate domains of hcp and fcc surface stacking. (b) Inset of the surface structure at the step edge facing hcp terrace regions: step atoms rearrange so as to form a close-packed planar surface, tilted by 28° with respect to the nominal [111] direction. (c) Profile of the simulated STM image across the hcp and fcc parts of the step, using a hemispherical tip of radius 2 \AA , together with the same image after removing convolution effects ($R = 0 \text{ \AA}$; see text for more details) and experimental results. (a) and (b) are taken from Ref. 9.

with objects of any shape yields minor modifications to the surface profile. In this section we present simulated STM images of a formate molecule (HCO) adsorbed on Pt(111),

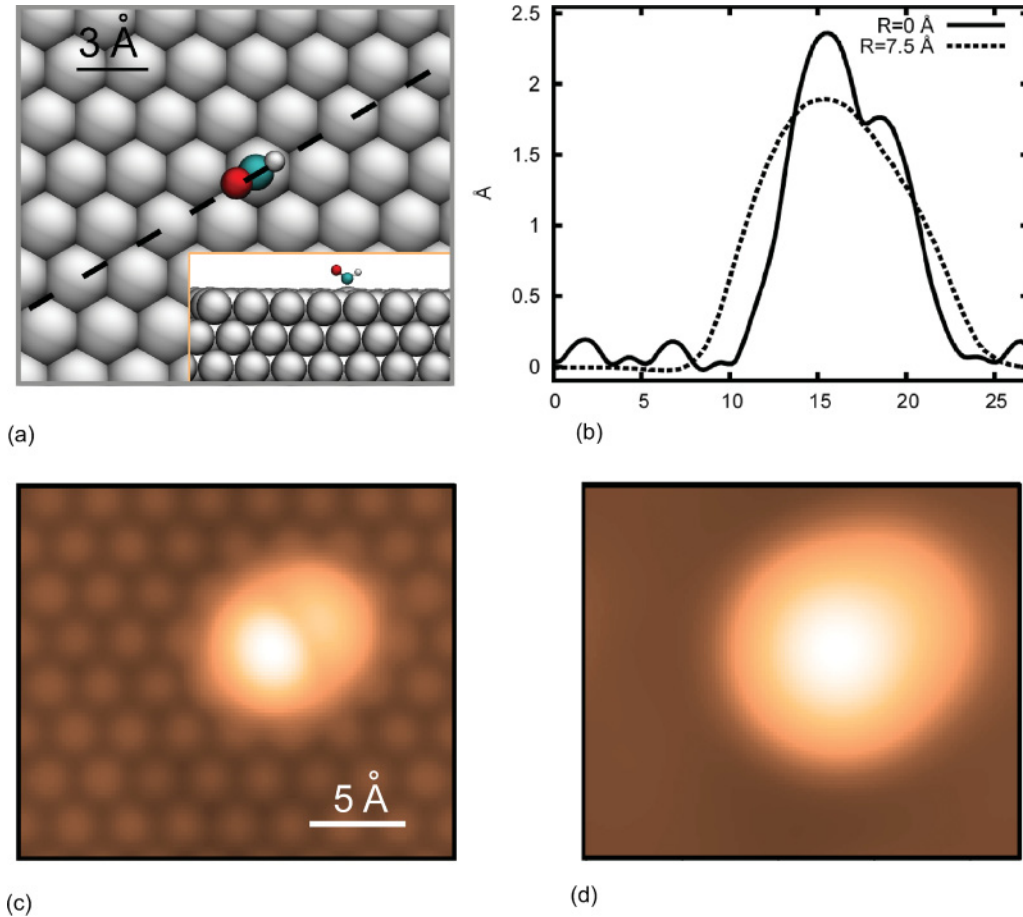


FIG. 5. (Color online) (a) Atomistic model of the HCO/Pt(111) system. H atom is white, C atom is medium gray (green online), and O atom is dark gray (red online). Pt atoms are represented as large white spheres. C is in the on-top position while the C-H and C-O bonds point to the hollow surface sites. The dotted line represents the direction of the line scan displayed in (b). In the inset of (a) a lateral view of the system is shown. (c),(d) STM images obtained using tips with $R = 0 \text{ \AA}$ (c) and $R = 7.5 \text{ \AA}$ (d). Protruding regions are associated with brighter colors.

under conditions of small tip-sample separation (Fig. 5). The HCO molecule presents typically a depression-protrusion pair in the STM appearance and it is interesting to see how this pattern is modified by tip-sample convolution effects. The adsorption process of HCO on Pt(111) has already been characterized theoretically,²⁵ where several possible geometries of adsorption have been compared. We optimized the structure using the procedure described in Sec. II. The initial condition was chosen to be the most stable configuration suggested in Ref. 25, with a C atom on top of a Pt surface atom and the H and O atoms pointing to the two hollow sites of the surface. After DFT relaxation the distance between the C atom and the underlying Pt atom is 1.96 \AA , the Pt atom being pulled out of the surface plane by about 0.2 \AA ; the C-O and the C-H distances are respectively 1.20 and 1.12 \AA , and the H-C-O angle is 122° . The STM images were simulated using a blunt tip (7.5 \AA), at a bias of -0.5 eV and a current of 100 nA . These conditions correspond experimentally to a situation of high current and small tip-sample distance [4.0 \AA according to Eq. (11)]. The simulated STM image appears very broad, the width at half height and the height being 10.3 and 1.9 \AA , respectively. These features are a consequence of using a large tip, smoothing out surface details also at conditions of high current. However,

by removing convolution effects as described previously, we obtain a surface pattern which appears qualitatively different: the width at half maximum decreases by 28% (7.5 \AA) and the height increases by 21% (2.4 \AA) with respect to the convoluted image, the molecule displays a depression-protrusion pair which closely resembles the HCO geometry, and atomistic resolution is achieved on the Pt substrate. Therefore the use of a blunt tip implies a considerable smoothing not only of the molecular corrugation but also of the whole STM image. The difference between the images taken with $R = 7.5 \text{ \AA}$ and $R = 0 \text{ \AA}$ tips is made large by the condition of high current, as opposed to the case of HBC on Cu(111) where the tip-sample distance was 3 \AA larger and the convolution effects less evident.

V. COMPARISON TO THE TH MODEL

In the previous section we compared images obtained, *within our model*, using several tip radii and showed the impact of convolution effects in the STM imaging. Using a pointlike tip ($R = 0 \text{ \AA}$) is equivalent, at our level of approximation, to modeling the tip as a single atom with *s*-orbital character. This is different from the TH approximation, which models the

tip as a macroscopic spherical potential well and describes its eigenstates as a single s wave. The results of the two approaches appear similar: both predict the STM image to be a contour of the sample LDOS. In the s -orbital model, however, this amounts to computing the LDOS at the position of the tip apex atom, whereas in the TH approximation the tunneling current is proportional to the sample LDOS at the center of the spherical well. Computation of the sample LDOS at the center of the well accounts for the lateral averaging of the tip as increasing the distance at which the LDOS contour is performed implies a smoother simulated STM image. In the SOC, broadening effects are accounted for by the explicit convolution of tip shape and LDOS. A comparison between the two methods can be performed by inspecting the tip LDOS of the respective tip models. It can be shown that, in the SOC model, the LDOS of the tip becomes proportional to the square of a single s wave in the limit of large distances from the tip surface or for small values of the tip radius. Under these conditions our approach and the TH modeling become equivalent. We have quantified the actual difference between STM images of the systems treated in the previous section, within the SOC and TH models. During the process of evaluation of the appropriate CLDOS for our model, the LDOS values at the center of the tips have also been computed. The corresponding LDOS isosurfaces represent the TH image suitable for comparison with our model. The comparison between our model and the TH model is shown in Fig. 6. Clearly, the profiles can be superimposed in the case of the Au(677) step, where the ratio between the tip radius R and the average tip-surface distance d is about 0.33. In the case of the HBC/Cu(111) system this quantity increases to 1.11 and therefore a larger difference between the profiles is expected. This can be verified by inspection of Fig. 6. A two-dimensional (2D) image comparison (Fig. 7) is provided in the case of the HCO/Pt(111) system, together with a scan line across the molecule (along the direction shown in Fig. 5). The ratio R/d is in this case 1.88 and a larger difference between the SOC and the TH models is expected. A close inspection of the 2D STM image reveals that the molecular protrusion appears more symmetric in the SOC simulation than in the TH one. This can be observed also in the line scan, where the tip height on the H atom is slightly enhanced in the SOC image. However, both the apparent width and height of the molecule are reproduced in a very similar way by the two approaches. The comparisons performed show that under typical experimental conditions our model and the TH approximation become equivalent. On the other hand the model proposed in this work has more flexibility in the choice of the tip geometry, as it allows simulations of STM images using an arbitrary tip shape. From a technical point of view our method requires a smaller convergence of the surface wave function in vacuum than the TH approximation. The largest contribution to the integral in (10) comes from the sample LDOS at regions where the tip is at its closest distance from the sample. Therefore the exact knowledge of the sample LDOS in the far vacuum is less critical than in the TH model, which requires the exact computation of the sample LDOS at the center of the tip. This can be an advantage of our approach in cases of DFT calculations using standard codes, which provide accurate sample states up to a limited distance from the surface.

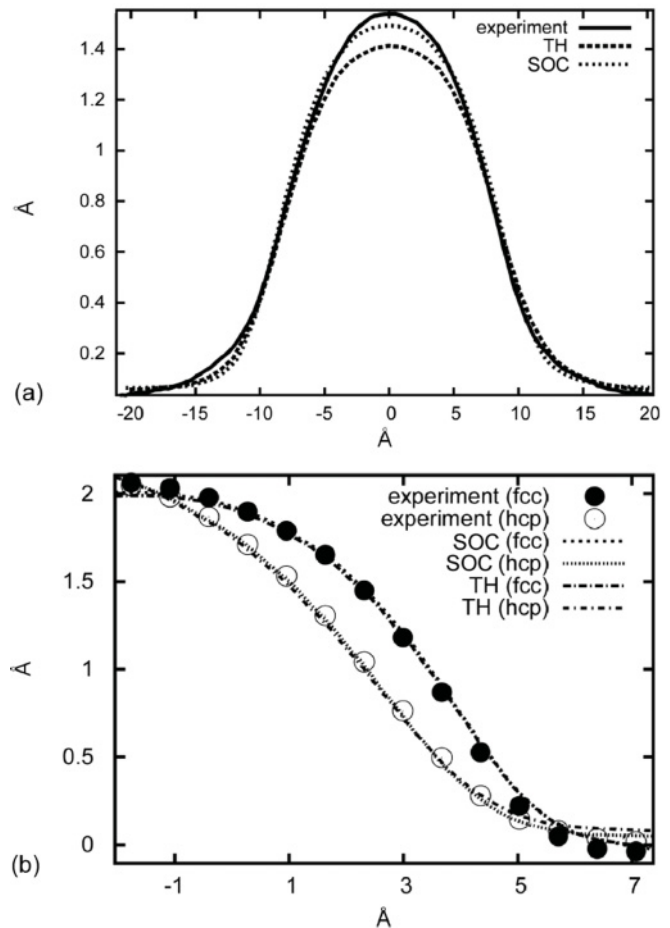


FIG. 6. The line profiles obtained with our model using a spherical tip and simulation parameters as specified in the text superimposed on the corresponding LDOS contour lines computed at the center of the sphere for (a) HBC on Cu(111) and (b) the Au(677) step profile.

VI. SIMPLE 1D MODEL OF THE SURFACE

The resolution of STM in the Tersoff-Hamann approximation has been thoroughly discussed with the help of simple one-dimensional models.²⁶ These investigations quantify the broadening effects of the tip in the Tersoff-Hamann approximation in the case of surfaces displaying defects with different dimensionality. It is seen that, while a step profile is simply smeared by the presence of the tip, a finite adsorbate has a decreasing apparent height as the tip-surface distance is increased. We are interested to quantify these effects in our model using other tip shapes than the spherical one. In the following we focus on a simple one-dimensional system imaged by a pyramidal-like tip. Here we consider two simple one-dimensional objects having the necessary properties to display dimensional effects in the STM imaging. We idealize these objects as a sharp step, infinitely extended in one direction (infinite object i) and described by the Heaviside function $g_i(x)$, and a localized surface defect (finite object f) corresponding to the combination of two Heaviside functions $g_f(x)$ (see Fig. 8). A correct quantum mechanical description of the electronic structure of objects i and f should predict a smearing of the LDOS isovalue profiles as the LDOS isovalue

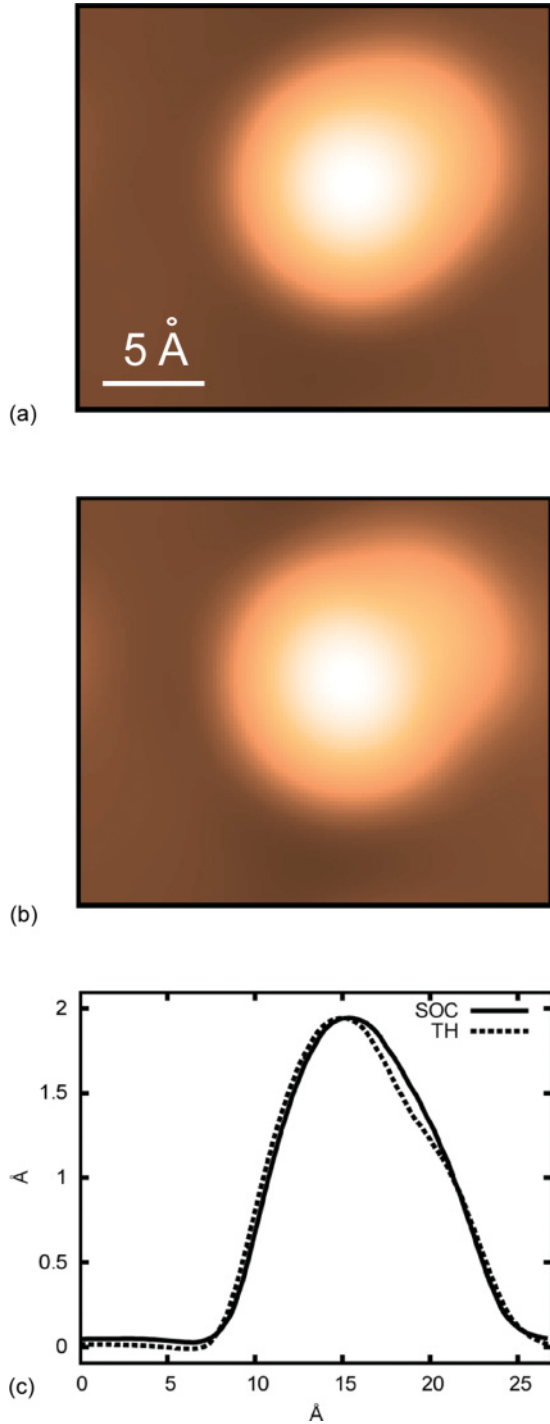


FIG. 7. (Color online) STM images obtained using the SOC model (a) and TH model (b), using a tip of radius $R = 7.5 \text{ \AA}$. Protruding regions are associated with brighter colors. (c) Corresponding line profiles taken across the molecule [along the line scan specified in Fig. 5(a)].

is decreased. However, we refer here to the condition of small tip-sample separation, where the profiles bear a close resemblance to the topography given by $g_i(x)$ and $g_f(x)$, as predicted by the model in Ref. 26. We therefore consider a simple toy model where the LDOSs of the two objects can be expressed as $\bar{\rho}_f(x,z) \propto e^{-\alpha[z-g_f(x)]}$ and $\bar{\rho}_i(x,z) \propto e^{-\alpha[z-g_i(x)]}$.

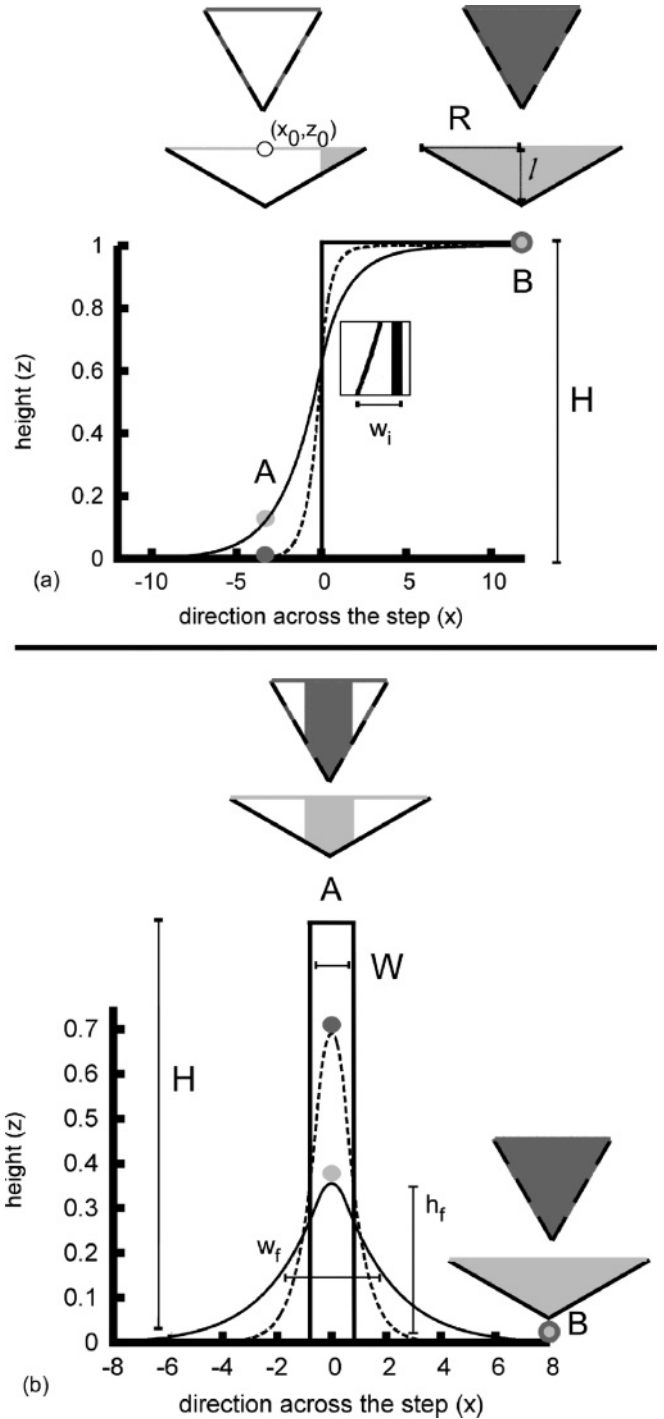


FIG. 8. Examples of the imaging of a finite and an infinite object using a blunt tip (solid line, $\omega = \sqrt{3}/2$) and a sharp tip (dashed lines, $\omega = 1/2$). The edge of the object is represented by thicker solid lines. Light (dark) gray dots specify the locations of the blunt (sharp) tip at two points (A,B) along the profiles. Within the volume occupied by the tip, filled domains correspond to regions where the LDOS of the isolated sample is largest.

The $\bar{\rho}$ functions can be inserted in Eq. (10) and the integration performed over the volume of the tip, which is described by the function $q(x-x_0)$. In order to make integrals exactly solvable we choose a pyramidal-like tip shape given by

$q(x - x_0) = l - \frac{l}{R}|x - x_0|$. The current value then reads

$$I(x_0, z_0) = I_0 \int_{x_0-R}^{x_0+R} dx \int_{z_0-q(x-x_0)}^{z_0} e^{-\alpha[z-g(x)]} dz, \quad (12)$$

where I_0 is a constant. Solving (12) for z_0 in the case of finite and infinite objects yields the isolevel expressions. If l and R are increased by keeping their ratio $R/l = \omega$ constant, the isolevels converge very rapidly to a final shape, since the density of states of the sample decreases at an exponential rate along the direction perpendicular to the surface. The solution is then taken in the limit of $l \rightarrow +\infty$, $R \rightarrow +\infty$ at constant ω . This allows simplification of the form of the isolevels and a description of the tip in terms of a single parameter, the tip width ω . The analytical expressions of the isolevels obtained are reported in (A2). In Fig. 8 we report the profiles calculated for the infinite and finite objects in the cases of a sharp ($\omega = 1/2$) and a blunt ($\omega = \sqrt{3}/2$) tip. It is noticeable that imaging the finite object with a blunt tip results not only in an increase of the apparent width of the object but also in a remarkable decrease of the apparent height. This can be explained by the fact that, if we increase the tip width by keeping the tip-surface distant constant, the tunneling current recorded at regions far away (region B, Fig. 8) from the localized defect increases more than above the defect itself (region A, Fig. 8). This is in turn due to the sample LDOS contained in the side regions of the tip in region B, which is larger than at region A. Therefore if the current has to be kept constant during the scan, larger tips have to go closer to the surface in region A, thus resulting in a smaller apparent height. From the knowledge of the isolevels' analytical form it is possible to obtain the apparent height (h_f, h_i) and the apparent width (w_f, w_i) of the defects, which are displayed in Fig. 8. While w_f is meant as the total width of the object at half apparent height, w_i refers to the width increase at half height with respect to the physical edge of the step [see the inset of Fig. 8(a)]. The form of these functions is given in (A2). For the infinite object, the apparent height is constant and equal to the physical height, while the apparent width increases linearly with ω . On the contrary the apparent width and height of the finite object appear to depend nonlinearly on ω as can be appreciated by inspection of the formulas in

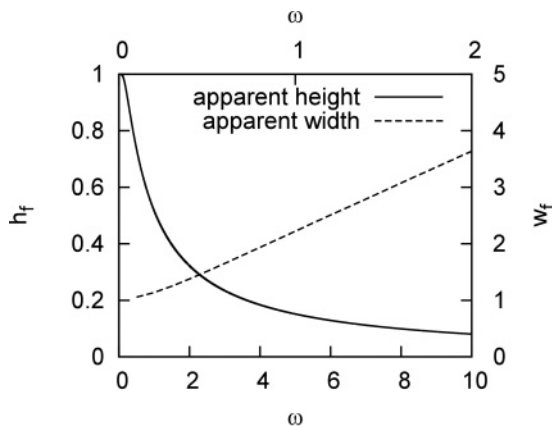


FIG. 9. Dependency of h_f and w_f on ω in the case of $H = W = \alpha = 1$. For an explanation of these quantities; see Fig. 8 and the text. Bottom x axis refers to h_f , while top x axis refers to w_f .

(A2). Because of the quite intricate form of w_f and h_f we plot these quantities over a range of ω for $H = W = \alpha = 1$ (see Fig. 9), in order to better visualize their behavior. The behavior of w_f is almost linear while h_f falls off rapidly with ω . Actually, in the limit of large ω , $w_f \propto \omega$ and $h_f \propto \frac{1}{\omega}$. The ω dependency of the apparent height results as the manifestation of a dimensionality-related effect, which arises in the case of STM images of localized defects.

VII. CONCLUSIONS

In this paper we have presented a generalization of the single- s -orbital model for the simulations of STM images, by describing the tip states in terms of a large number of s -orbital scatterers centered on the tip atoms. By averaging the STM current over the tip atomic configurations which are compatible with a given tip shape and using the incoherent sum approximation, we have shown that the resulting current intensity is proportional to the convolution product of the system LDOS with a step function which is defined by the effective tip volume. The results apply to tips of arbitrary shape. The application of the method to three cases of current scientific interest, namely, a hexaperihexabenzocoronene molecule adsorbed on Cu(111), a reconstructed Au(111) surface, and a HCO molecule adsorbed on Pt(111), shows that corrections due to the tip size can be effectively taken into account by the approach presented in this work. These effects correspond to a loss of resolution of the STM image summing up to topography broadening dependent on the tip-sample distance. The tip-induced image broadening was further quantified with the use of a simple 1D surface model and a pyramidal-like tip, where we showed, by analytically deriving the surface profiles, that an increase of the tip size leads to a smearing of the surface step profile and a reduction of the height of finite objects. In the case of spherical tips, STM images obtained within our approach and the TH model are equivalent under typical experimental conditions. However, our method allows simulation of STM images using tips of any shape at a very moderate computational cost, which differs negligibly from that demanded by the TH modeling. Finally the possibility of consistently defining the effective cross-sectional area for spherical and other tip shapes allows the use of one-dimensional models for the estimation of the tunneling current, thereby offering a simpler framework for the calculations with respect to models requiring the exact three-dimensional geometry of the junction.

ACKNOWLEDGMENTS

We thank Dr. Paolo Ferriani and Dr. Howard Mizes for their constructive comments on the manuscript. We acknowledge the Swiss Center for Scientific Computing for computational resources and the Swiss National Science Foundation and the Alexander von Humboldt Foundation for financial support.

APPENDIX A

Assuming that the LDOS of a flat surface can be represented by $f(z) \propto e^{-kz}$, a flat electrode of surface S at distance d from

the sample records the following intensity current, according to Eq. (10):

$$I = CS \int_d^\infty e^{-kz} dz \quad (\text{A1})$$

where C represents the proportionality constant. For a hemispherical electrode of radius R we have

$$I = \pi C e^{-kd} \int_0^R e^{-kz} (2Rz - z^2) dz. \quad (\text{A2})$$

Equating Eqs. (A1) and (A2) we obtain the relationship

$$S(R) = \pi k^{-2} [(2kR - 2) - e^{-kR} (k^2 R^2 - 2)], \quad (\text{A3})$$

which can be used to estimate the effective cross-sectional area of a hemispherical tip of radius R .

APPENDIX B

Hereafter we report the explicit expression of the isolevels for the finite and infinite objects of the exactly solvable 1D model:

$$z_i = \begin{cases} \frac{1}{\alpha} \ln \frac{I_0 \omega}{I} [A + B e^{\frac{\alpha x}{\omega}}] & \text{if } x \leq 0, \\ \frac{1}{\alpha} \ln \frac{I_0 \omega}{I} [C - B e^{-\frac{\alpha x}{\omega}}] & \text{if } x \geq 0, \end{cases}$$

$$z_f = \begin{cases} \frac{1}{\alpha} \ln \frac{I_0 \omega}{I} [A + 2B e^{\alpha x / \omega} \sinh(\frac{\alpha W}{2\omega})] & \text{if } x \leq -W/2, \\ \frac{1}{\alpha} \ln \frac{I_0 \omega}{I} [C - 2B e^{-\alpha W / 2\omega} \cosh(\frac{\alpha x}{\omega})] & \text{if } x \leq |W/2|, \\ \frac{1}{\alpha} \ln \frac{I_0 \omega}{I} [A + 2B e^{-\alpha x / \omega} \sinh(\frac{\alpha W}{2\omega})] & \text{if } x \geq W/2. \end{cases}$$

I is the constant current value, I_0 is the proportionality constant defined in Eq. (12), α is the inverse decay length of $\bar{\rho}$ in vacuum, W is the width of the finite object, and ω is the tip width; other constants are $A = 2\alpha^{-1}$, $B = (e^{\alpha H} - 1)\alpha^{-1}$, and $C = A e^{\alpha H}$. H is the height of the objects.

The apparent height h of the objects can be calculated from the above profiles as $h = \frac{z(\infty) + z(-\infty)}{2}$. The width w is obtained by substituting h for z in the above equations and solving for $|x| = w_i$ for infinite objects and for $|x| = \frac{1}{2}w_f$ for finite objects. This gives

$$h_i = H,$$

$$w_i = \frac{\omega}{\alpha} \ln \left[\frac{B}{\sqrt{AC} - A} \right],$$

$$h_f = \frac{1}{\alpha} \ln \left[\frac{C - 2B e^{-\alpha W / 2\omega}}{A} \right], \quad (\text{B1})$$

$$w_f = \frac{2\omega}{\alpha} \ln \left[\frac{2B \sinh[\frac{\alpha W}{2\omega}]}{\sqrt{AC} - 2AB e^{-\alpha W / 2\omega} - A} \right].$$

*roberto.gaspari@empa.ch

†Present address: Institut de Science et d'Ingenierie Supramoleculaire (ISIS) University of Strasbourg 8, allée Gaspard Monge, F-67000 Strasbourg, France

‡Also at Department of Chemistry and Biochemistry, University of Bern, Freiestrasse 3, 3012 Bern, Switzerland.

§daniele.passerone@empa.ch

¹A. Gottlieb and L. Wesoloski, *Nanotechnology* **17**, R57 (2006).

²J. Bardeen, *Phys. Rev. Lett.* **6**, 57 (1961).

³W. Hofer and J. Redinger, *Surf. Sci.* **447**, 51 (2000).

⁴W. A. Hofer, A. S. Foster, and A. L. Shluger, *Rev. Mod. Phys.* **75**, 1287 (2003).

⁵J. Tersoff and D. R. Hamann, *Phys. Rev. B* **31**, 805 (1985).

⁶C. J. Chen, *Phys. Rev. B* **42**, 8841 (1990).

⁷J. VandeVondele *et al.* [<http://cp2k.berlios.de/>].

⁸J. VandeVondele and J. Hutter, *J. Chem. Phys.* **127**, 114105 (2007).

⁹R. Gaspari, C. A. Pignedoli, R. Fasel, M. Treier, and D. Passerone, *Phys. Rev. B* **82**, 041408 (2010).

¹⁰N. Gonzalez-Lakunza, I. Fernandez-Torrente, K. J. Franke, N. Lorente, A. Arnau, and J. I. Pascual, *Phys. Rev. Lett.* **100**, 156805 (2008).

¹¹C. Corriol, V. M. Silkin, D. Sanchez-Portal, A. Arnau, E. V. Chulkov, P. M. Echenique, T. vonHofe, J. Kliever, J. Kroger, and R. Berndt, *Phys. Rev. Lett.* **95**, 176802 (2005).

¹²R. Mazzarello, A. D. Corso, and E. Tosatti, *Surf. Sci.* **602**, 893 (2008).

¹³V. Chis and B. Hellsing, *Phys. Rev. Lett.* **93**, 226103 (2004).

¹⁴S. Grimme, *J. Comput. Chem.* **27**, 1787 (2006).

¹⁵C. Di Valentin, *J. Chem. Phys.* **127**, 154705 (2007).

¹⁶M. Rohlfing, R. Temirov, and F. S. Tautz, *Phys. Rev. B* **76**, 115421 (2007).

¹⁷S. Monturet, Ph.D. thesis, University of Toulouse, 2008.

¹⁸M. Bocquet and B. Wang, *Prog. Surf. Sci.* **85**, 435 (2010).

¹⁹H. A. Mizes, S. I. Park, and W. A. Harrison, *Phys. Rev. B* **36**, 4491 (1987).

- ²⁰S. Watanabe, M. Aono, and M. Tsukada, *J. Vac. Sci. Technol. B* **12**, 2167 (1994).
- ²¹N. D. Lang, *Phys. Rev. B* **34**, 5947 (1986).
- ²²G. Simmons, *J. Appl. Phys.* **34**, 1793 (1963).
- ²³F. Jäckel, M. D. Watson, K. Müllen, and J. P. Rabe, *Phys. Rev. Lett.* **92**, 188303 (2004).
- ²⁴S. Rousset, V. Repain, G. Baudot, Y. Garreau, and J. Lecoœur, *J. Phys.: Condens. Matter* **15**, S3363 (2003).
- ²⁵T. Roman, H. Nakanishi, and H. Kasai, *Phys. Chem. Chem. Phys.* **10**, 6052 (2008).
- ²⁶W. Sacks, S. Gauthier, S. Rousset, J. Klein, and M. A. Esrick, *Phys. Rev. B* **36**, 961 (1987).